Wear 458-459 (2020) 203403

Contents lists available at ScienceDirect

Wear

journal homepage: http://www.elsevier.com/locate/wear

Numerical simulation of tool wear in drilling Inconel 718 under flood and cryogenic cooling conditions

A. Attanasio [a,*], E. Ceretti [a], J. Outeiro [b], G. Poulachon [b]

[a] University of Brescia, Department of Mechanical and Industrial Engineering, Via Branze 38, 25123, Brescia, Italy
[b] Arts et Métiers Institute of Technology, LABOMAP, HESAM University, Rue Porte de Paris, F-71250, Cluny, France

ARTICLE INFO

Keywords:
FEM simulation
Drilling
Tool wear
Cryogenic cooling
Inconel 718

ABSTRACT

This paper aims to model and simulate tool wear in drilling of Inconel 718 under two different cooling conditions, using an innovative numerical procedure. Although tool wear models can be implemented in most of finite element analysis (FEA) software to calculate the tool wear rate, there is a great limit due to the inability of all these software to update the geometry of the worn tool. In order to overcome this limitation, a subroutine able to modify the tool geometry based on a given tool wear model was developed and implemented in DEFORM 3D, an implicit FEA software. Experimental tests were performed to measure tool wear in drilling using conventional metal working fluids (MWF) and liquid nitrogen (LN_2) cooling. Experimental data were used to calibrate the tool wear model and to validate the drilling models. A comparison between simulated and measured results demonstrated the suitability of the developed drilling model to predict tool wear under both MWF and LN_2 cooling conditions. Therefore, the developed model can be efficiently used to evaluate the influence of the cutting conditions (including cooling conditions) on tool wear, minimizing the number of expensive and time-consuming tool wear tests.

1. Introduction

Nickel-based alloys are well-known and interesting materials due to their chemical, physical and mechanical properties. This family of alloy is characterised by high melting temperature, great resistance to corrosion and creep phenomena, high wear resistance and high strength at elevated temperature [1]. Therefore, these materials are widespread in advanced manufacturing industries (such as: automotive, aerospace, chemical, energy, and medical) for manufacturing components operating in corrosive environment and/or under high thermal and mechanical loadings. Some examples of products made of Nickel-based alloys are in general critical jet engine components, power generation systems, components of nuclear reactors, valves and distributors for chemical and petrochemical installations. The main drawback of these alloys is their poor machinability due to their enhanced mechanical properties. Therefore, high tool wear and low productivity may increase the machining costs up to five times when compared to plain carbon steel [2,3]. The machining costs also increase because of the high surface integrity requirements of critical components made of Nickel-based alloys [4]. Studies on this topic demonstrated that inadequate machining conditions are detrimental for the final surface integrity [5]. In particular, tool wear must be carefully monitored to avoid excessive surface damages and tensile residual stresses in the final part [6]. Cutting tool materials play an important role in machining such materials. For instance, polycrystalline cubic boron nitride (PCBN) inserts guarantee low tool wear and high productivity with respect to physical vapour deposition (PVD) coated cemented carbide [7,8]. It was demonstrated that tool life can be also increased using assisted machining solutions [9], such as high-pressure jet [10] and cryogenic cooling [11].

Due to its relevance in cutting, many researchers have focused their attention on modelling tool wear. Different wear models were developed depending on the wear mechanisms involved in cutting (adhesion, abrasion [12–14], diffusive wear [14–18], corrosion). All these models describe the wear evolution throughout analytical equations, which estimate the wear rate in function of process parameters [13,19,20], work material properties, tool material properties, and tool geometry [15,16,21].

The first finite element (FE) model of cutting was developed in the 70's [22]. This FE model was used to analyse the soil performance under the action of the blade and to optimise the rake angle of the cutting tool. The development of FE models for metal cutting starts in the 80's and

* Corresponding author.
E-mail address: aldo.attanasio@unibs.it (A. Attanasio).

https://doi.org/10.1016/j.wear.2020.203403
Received 7 February 2020; Received in revised form 18 June 2020; Accepted 2 July 2020
Available online 25 July 2020

90's [23]. Due to the low computational performance of the workstations, the finite element analysis (FEA) was limited to the simulation of the orthogonal cutting process, which can be modelled as two dimensional (2D). In particular, 2D FE models were developed to study the influence of tool geometry and cutting regime parameters on chip flow [24], cutting force [25] and to study the fatigue failure mechanisms of tools [26]. In this period, very few three-dimensional (3D) models of oblique cutting [27,28] can also be found in literature. The increase of computational performance and the development of new solver algorithms led to a wide spread of FEM-based simulations of the metal cutting process [29,30]. 3D FE models were developed to simulate turning [31], milling [32] and drilling [33] operations. These models are used to predict the metal cutting performance (forces, temperatures, etc) and the surface integrity. Attanasio et al. [34] developed a 3D model for predicting the surface integrity in turning. The influence of consecutive passes was studied. Umbrello et al. [35] studied the influence of the coefficient of the constitutive model on the FEM results. Pujana et al. [36] used FE analysis for the inverse identification of the parameters of the material constitutive model. The influence of tool geometry and tool coating on the temperature distribution in the tool was analysed by M'Saoubi et al. [37]. Klocke et al. [38] developed an FE model to investigate the high speed machining (HSM) of orthogonal cutting demonstrating the ability of this technique in describing the HSM. Rotella et al. [39] and Jafarian et al. [40] developed and tested a FE model for the simulation of microstructural changes of the workpiece material. The FEA was also used to simulate the tool run-out effect on micromilling as reported by Attanasio et al. [41]. Sai Venkatesh et al. [42] and Xie et al. [43] used 2D FE simulation to study the influence of tool wear in orthogonal cutting.

So far, very few metal cutting models are available in the literature for predicting tool wear in real (3D) machining operations [44], and nothing for drilling. Therefore, the main objective of this paper is to develop a simulation strategy to simulate tool wear in drilling considering the tool geometry update. All the FEM software used in cutting simulation can estimate the tool wear rate, but none of them are able to modify/update the tool geometry based on the calculated tool wear. Attanasio et al. [44] developed a simulation procedure to update the tool geometry using customised user-routines able to rebuild the geometry of the worn tool by modifying its mesh. Recently, some FEA software (e.g. Deform) implemented methods to automatically modify the geometry of forging dies considering the tool wear rate. However, the automatic update of the tool geometry in machining considering the wear rate is not yet available in commercial FEA software.

The novelty of this research work is the possibility of simulating drilling operations considering the actual worn tool geometry. This was done by developing a new user-routine based on an existing one developed for tool wear simulation in turning [45,46]. In this user-routine a new algorithm for the tool geometry update was developed. The algorithm identifies small local wear volumes (LWV) of material lost to correctly define the geometry of the worn tool. The predicted results in terms of tool wear evolution and drill torque were compared with those obtained experimentally by Outeiro et al. [47] in drilling Inconel 718 drilling using both conventional Metal Working fluids (MWF) and cryogenic cooling conditions. This comparison permitted to conclude that the proposed simulation strategy gives the possibility to properly simulate the tool wear in drilling Inconel 718 under both cooling conditions.

2. Experimental tests

Drilling tests were carried out to obtain the tool wear curves and other relevant information to setup the cutting tool wear model. A description of the experimental drilling tests and corresponding results is detailed by Outeiro et al. [47]. In particular, tool wear tests were performed on a CNC milling machine (DMG model DMU 65V) equipped with piezoelectric dynamometer for force/torque measurement. Workpieces in Inconel 718 solution-treated and age-hardened (44 HRC) were used in the drilling tests. Table 1 and Table 2 summarise respectively the chemical composition and the main mechanical properties of Inconel 718 as certificated by the material supplier.

Standard coated (TiAlN coating) cemented carbide twist drills were chosen to perform the drilling tests. It is worth pointing out that the drills selected for these tests are designed to work with high pressure metal working fluid (MWF), delivered to the cutting zone through the internal cooling channels of the drill. Drill geometry was inspected according to the ISO 3002–1/2 and DIN 1414–1/2 standards, using both ZOLLER Genius3/3DCheck and ALICONA InfiniteFocus. These devices permitted to scan the tool geometry, and to generate the drill CAD model for the numerical simulations. Drill geometry is summarised in Table 3.

The tool wear tests were performed under cryogenic (LN_2) cooling and conventional MWF conditions. LN_2 was delivered to the cutting zone at a pressure of 10 bars. A MWF composed by 5% of synthetic fluid (VULSOL 5000 S from TOTAL) mixed with water was delivered to the cutting zone with a pressure of 20 bars.

The optimal cutting conditions for each cooling strategy were obtained applying the concept of minimal specific cutting force, according to NF E66-520 standard. Table 4 shows the optimal cutting condition defined for each cutting fluid.

During the tests, tool wear parameter VB and drilling torque were measured. The tool wear was measured using the ALICONA InfiniteFocusSL, an optical 3D measurement system, which guarantees a measuring accuracy of 0.5 μm. The torque was measured by a Kistler piezoelectric dynamometer (model 9123C) which guarantees a measuring accuracy of 0.2 Nm. The natural frequency of the dynamometer is equal to 2 kHz. The frequencies of the force signals of each cutting conditions are respectively equal to 8.8 Hz for LN_2 and to 21.2 Hz for MWF. These being values lower than the natural frequency of the dynamometer, the measured values can be considered reliable.

3. Tool wear modelling and simulation

3.1. FE model of drilling

FE simulations of Inconel 718 drilling were conducted on Deform3D (Scientific Forming Technologies Corporation, Ohio), a commercial FEA software. Fig. 1a shows the geometry and mesh of the model, which includes a deformable workpiece and a rigid tool.

The workpiece geometry was a cylinder with a hole reproducing the profile of the drill. The CAD model was meshed with more than 100 000 tetrahedral elements. The minimum and the maximum element sizes were respectively set equal to 0.03 mm and 0.6 mm. The highest mesh density region was set on the contact zone between tool and workpiece in order to ensure a good mesh definition in the cutting zone (Fig. 1a). The thermo-visco-plastic behaviour of the Inconel 718 was selected from the material database of Deform 3D. The flow stress was obtained from material characterization tests performed by the Aerospace Manufacturing Technologies of the National Research Council of Canada for the Scientific Forming Technologies Corporation (the developer of DEFORM). The flow stress curves of Inconel 718 at different strain rates and temperatures are shown in Fig. 2a and Fig. 2b, respectively.

The tool was meshed with more than 340 000 tetrahedral elements setting a minimum element size of 0.03 mm and a maximum element size of 0.5 mm. A high mesh density was used around the cutting edge in order to reproduce its exact geometry and also to better represent the geometry of the worn tool (Fig. 1b). The physical, thermal and mechanical properties of the tool (substrate and coating) were selected from Deform3D database. Table 5 summarises these properties.

The tool-workpiece and tool-chip contacts were represented by Eq. (1),

$$\tau_f = m \cdot k \tag{1}$$

Table 1
Chemical composition of Inconel 718 in weight percentage.

Ni	Cr	Fe	Mo	Nb	Co	Mn	Cu
50.0–55.0	17.0–21.0	17	2.8–3.3	4.75–5.5	<1.0	<0.35	<0.3
Al	Ti	Si	C	S	P	B	
0.2–0.8	0.65–1.15	<0.35	<0.08	<0.015	<0.015	<0.006	

Table 2
Mechanical properties of Inconel 718.

Tensile Strength, Ultimate	min. 1375 MPa
Tensile Strength, Ultimate at 650 °C	min. 1100 MPa
Tensile Strength, Yield	min. 1100 MPa
Tensile Strength, Yield at 650 °C	min. 980 MPa
Elongation at Break	min. 25%
Elongation at Break at 650 °C	min. 18%

where τ_f is the tangential stress at the contact interface, k is the shear yield stress and m is the shear friction factor.

The values of the shear friction factor for each cooling condition were determined through tribological tests (Table 6).

A thermo-mechanical analysis was performed. The determination of the heat exchange among tool, workpiece and cutting fluid is very critical for an accurate prediction of the temperature distribution in the tool and workpiece. It is possible to manage the heat transfer among tool, workpiece and cutting fluid through the cutting fluid temperature (T_f), heat conduction coefficient (h_{cond}) across the tool-workpiece and tool-chip interfaces and heat convection coefficient (h_{conv}) with the cutting fluid. In metal cutting simulation, a high value of h_{cond} [48] is often used to reach the thermal steady state in a very short time. For this reason, this coefficient was set equal to 10^5 kW/(m^2 K). The determination of h_{conv} is difficult, in particular under cryogenic cooling conditions, since it depends on several factors [49,50]. This coefficient was determined by Outeiro et al. [47] for both LN_2 and conventional MWF. Their values are presented in Table 6.

3.2. Procedure for tool wear simulation

3.2.1. General description

The flowchart of Fig. 3 shows the developed procedure to perform tool wear simulations. Before running the user-routine to simulate the tool wear (grey rectangle in Fig. 3), it is necessary to run simulations to reach the force and temperature steady state during the drilling process. These simulations permit to calculate the temperature distribution in the cutting zone (tool, workpiece and chip), the distribution of the contact pressure between the tool and the chip, and the sliding velocity of the chip on the tool rake face.

Therefore, first step of the procedure aims to reach both mechanical and thermal steady-states. To reach the mechanical steady state, a Lagrangian incremental (IL) simulation is run. The mechanical steady-state is reached when a sufficient chip is formed, and the tool-chip contact length remains constant (i.e. the chip is curved and starts to separate from the tool rake face). Under these conditions, the drilling torque is constant. Once the mechanical steady-state is reached, the simulation must be switched from Lagrangian incremental to Arbitrary-Lagrangian-Eulerian (ALE). ALE formulation requires specific boundary conditions that include the definition of proper free surfaces, corresponding to the end surfaces of the chip, and proper thermal boundary

Table 4
Cutting conditions used in drilling.

Fluid	Pressure (bar)	Cutting speed, V_c (m/min)	Feed, f (mm/rev)
LN_2	10	10	0.11
MWF	20	24	0.11

Table 3
Drill geometry according to the ISO 3002–1/2 and DIN 1414–1/2 standards.

Parameter	Value	Parameter	Value	Parameter	Value	Parameter	Value
drill diameter	12.015 mm	point angle	143.4°	chisel edge centrality	0.013 mm	normal rake angle	−10°–32°
back taper	0.09°	drill runout	0.007 mm	web thickness	0.173 mm	normal clearance angle	10°–18°
helix angle	30°	chisel edge angle	56.7°	gash face angle	64°	average edge radius	55 μm
margins width	0.837 mm	chisel edge length	0.397 mm	gash radius	1.420 mm		

Standard deviation of length measurement (3 repetitions): ±0.5 μm.

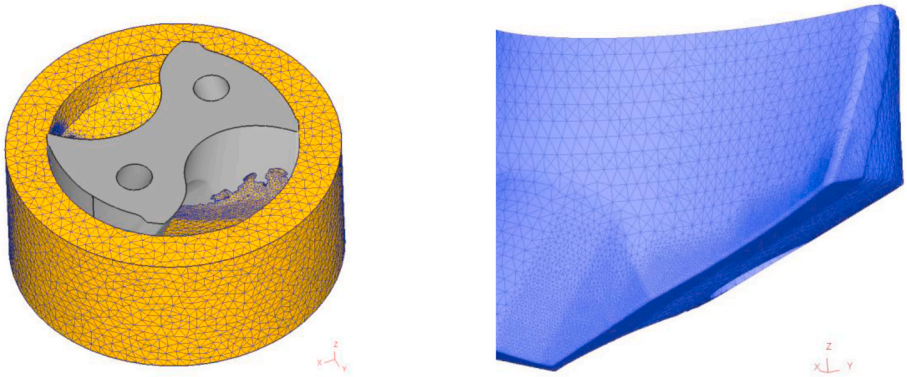

(a) (b)

Fig. 1. a) 3D FE model of drilling and b) detail of the mesh on the drill cutting edge.

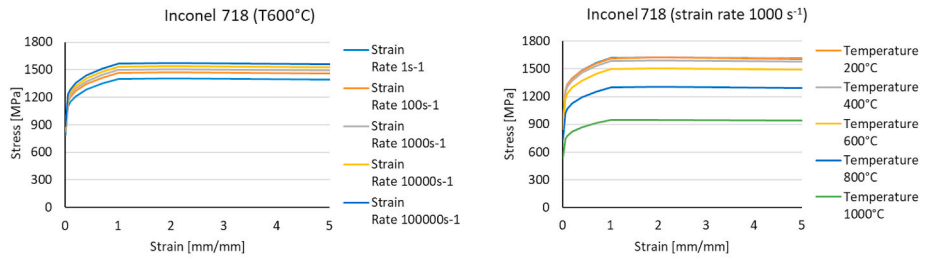

Fig. 2. Flow stress curves of Inconel 718 at a) several strain rates and b) several temperatures.

Table 5
Physical, thermal and mechanical properties of the tool (subtract and coating).

Parameter	Substrate (WC/Co)	Coating (TiAlN)
Thermal conductivity	59 N/s/C	30 N/s/C
Heat capacity	15 N/mm^2/C	15 N/mm^2/C
Emissivity	0.7	0.7
Thermal expansion	5e-06 C^{-1}	8e-06 C^{-1}
Density	15.7 g/cm^3	5.1 g/cm^3
Young's modulus	650000 MPa	448000 MPa
Poisson's ratio	0.25	0.23

Table 6
Shear friction factors and heat convection coefficients for MWF and LN_2 [47].

Cutting fluid	m	h_{conv}	T_f
MWF	0.10	0.930 kW/(m2 K)	20 °C
LN_2	0.25	6.270 kW/(m2 K)	−170 °C

conditions. At this stage, both cutting torque, and heat flow are constant as shown in Fig. 4.

Once the process steady state is reached, it is possible to simulate the tool wear. The second step is an iterative strategy (Fig. 3), repeated until reaching the final drilling time (t_{end}). At each iteration the incremental wear (ΔVB_i) is calculated for all the nodes of the tool cutting edge. First, it is necessary to set the discretisation time (Δt in Figs. 3 and 5). This time corresponds to the interval of time used to measure the tool wear experimentally. This time is used by the user-routine to calculate the tool wear increment (ΔVB_i) as described below. According to the experimental tests, the discretisation time was set equal to 30 s.

The computational time needed to run a of simulation of 15 min of cut is close to 90 h.

The tool wear rate model must be carefully selected, since this model strongly affects the simulation results. The core of this procedure is the user-routine, which allows to update the tool geometry according to the calculated tool wear rate. For this purpose, a new user-routine (Fig. 5) was developed for drilling, based on an existing one developed to simulate tool wear in turning [44,45].

When the user-routine is executed the tool wear rate distribution on the cutting edge is calculated (Step 2.1 in Fig. 5). Considering the steady state obtained from Step 1 and the selected tool wear model, the developed algorithm calculates the tool wear rate value of each node of the cutting edge.

Therefore, the user-routine can calculate the increment of the tool wear (ΔVB_i) for the iteration using Eq. (2).

$$\Delta VB_i = \frac{\partial W(t_i)}{\partial t}\cdot\Delta t + VB_0 \qquad \forall n \in [1, N] \tag{2}$$

where i is the iteration number, n is the node number, N is the total node number of the cutting edge, t_i is the current time, ΔVB_i is the flank wear increment of the current iteration, $\frac{\partial W(t_i)}{\partial t}$ is the tool wear rate at the current time and Δt is the discretisation time. VB_0 is set equal to the initial tool wear at the first iteration (for $i = 1$) and zero after the first iteration (for $i > 1$).

3.2.2. Empirical model of tool wear rate

Fig. 6 shows the results of the tool wear tests for both cryogenic cooling and MWF conditions obtained by Outeiro et al. [47]. Observing this figure, it is possible to identify the typical trend characterising the tool flank wear VB curves as described in several publications [51–53].

For both cooling condition, the collected data show a very short duration of the first region (primary [51,52] or running-in Ref. [53] wear) of only 30 s. This region is characterised by an accelerated wear of the tool and it seems that the cooling condition does not affect its duration. After 30 s of cutting, the drills showed a flank wear equal to 0.078 mm and 0.085 mm for LN_2 and MWF, respectively. The second region (steady state wear [51–53]) is the operating region of the tool and it is characterised by constant and progressive tool wear. When drilling under cryogenic cooling condition this region has a duration of only 8 min; while under MWF this duration is greater than 20 min. Concerning the third region (tertiary [51,52] or rapid [53] wear), this region is not observable for MWF cooling condition (Fig. 6b), while it is evident for cryogenic cooling (Fig. 6a). This is because, according to ISO standards [54–56], it was decided to stop the drilling tests once reached the mean flank wear limit of 0.3 mm. To conclude, the best tool life in drilling Inconel 718 is achieved using MWF. This result was expected, since the geometry/material of the drill was designed to work under MWF conditions.

The empirical models of tool wear rate for cryogenic cooling and MWF were obtained from the experimental tool wear curves shown in Fig. 6. Equations (3) and (4) report these wear rate models in function of cutting time for both cryogenic cooling and MWF, respectively. These models were obtained by fitting the experimental data for the steady state regions using a second order polynomial function and finding the derivatives of these functions.

$$\frac{\partial W}{\partial t} = -0,0004\cdot t + 0,0153;\ VB_0 = 0.078\ mm \tag{3}$$

$$\frac{\partial W}{\partial t} = 0,0034\cdot t + 0,0087;\ VB_0 = 0.085\ mm \tag{4}$$

The analysis was limited to the second tool wear region in order to consider just the operating region of the tool.

A preliminary iteration was run to generate an initial tool geometry including VB_0. The tool wear value set in the algorithm during this first iteration corresponds to the flank wear value measured at the end of the primary wear region.

The choice to focus on the steady state wear region is not due to any kind of limitation of the simulation procedure. This procedure can also be applied to the primary and the tertiary wear regions. To do it, it is just necessary to define a suitable tool wear model that includes also these two regions. It was decided to limit the analysis to the second tool wear region because the first region showed a very short duration (lower than

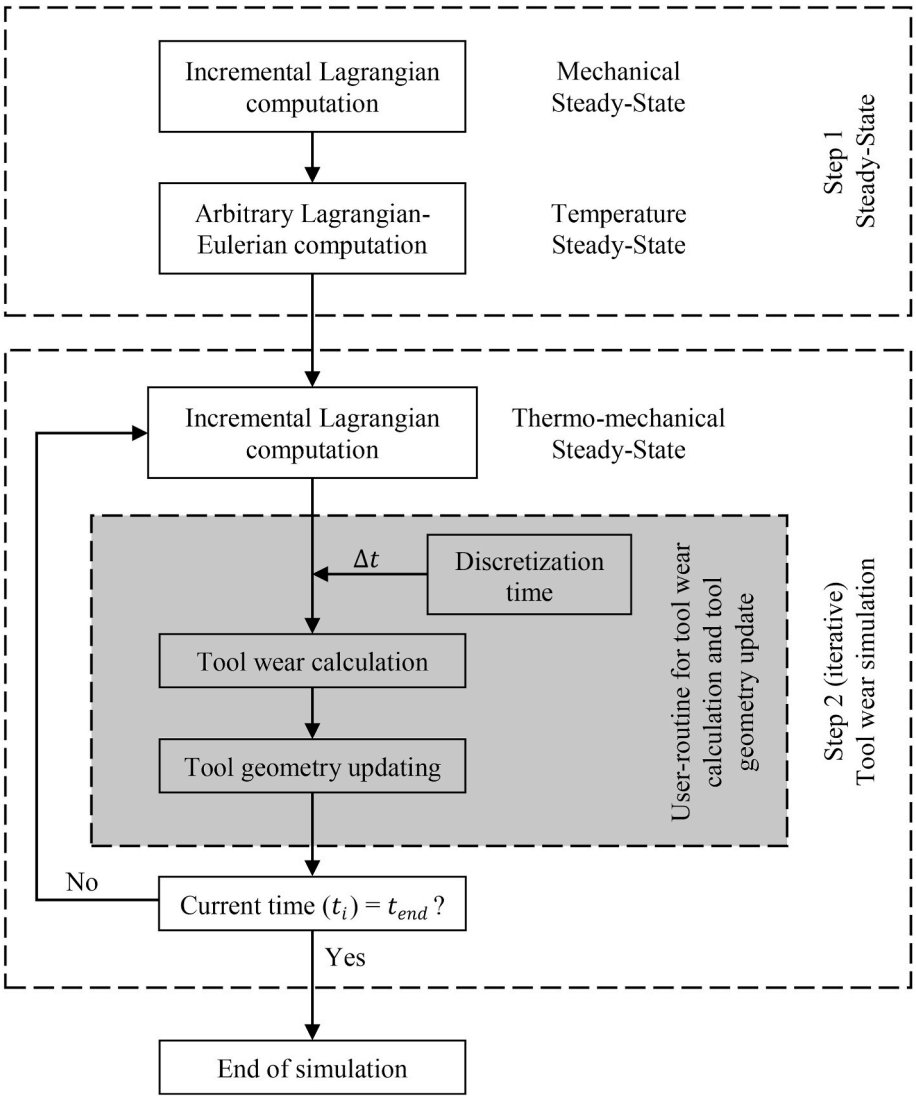

Fig. 3. Simulation procedure for tool wear prediction with tool geometry updating.

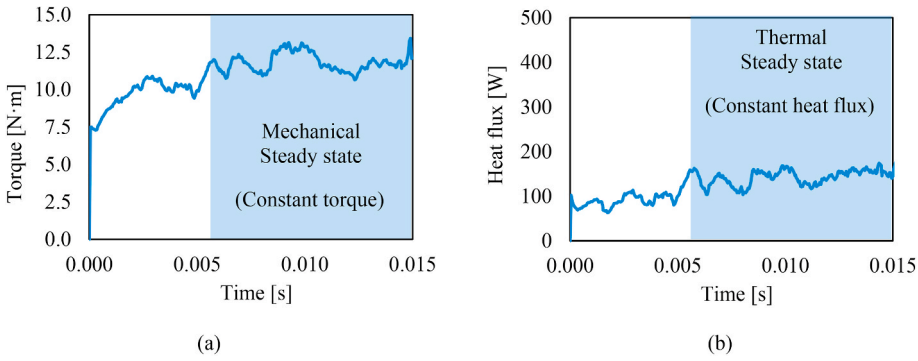

Fig. 4. Mechanical a) and thermal b) steady state regime. (MWF, VB = 0.085 mm).

30 s) for both the cooling conditions, while the third region was only observed under LN_2 cooling condition. Moreover, the objective of this work is to demonstrate the validity, the reliability, and the accuracy of the proposed procedure to simulate tool wear in drilling.

3.2.3. *Procedure to update the geometry of the worn tool*

The value of ΔVB_i (Fig. 5) is used for the geometrical reconstruction of the wear profile along the cutting edge. The complexity of the drill geometry makes this step complex. Fig. 7 shows that the flank wear of a worn drill is not constant along the tool cutting edge. Due to the increase of the cutting speed from the drill centre to the drill periphery, the flank wear linearly increases from the chisel edge to the begin of the curved part of the cutting edge (Fig. 7a). Then, tool wear remains constant along the curved part of the cutting edge until the drill margins (Fig. 7b).

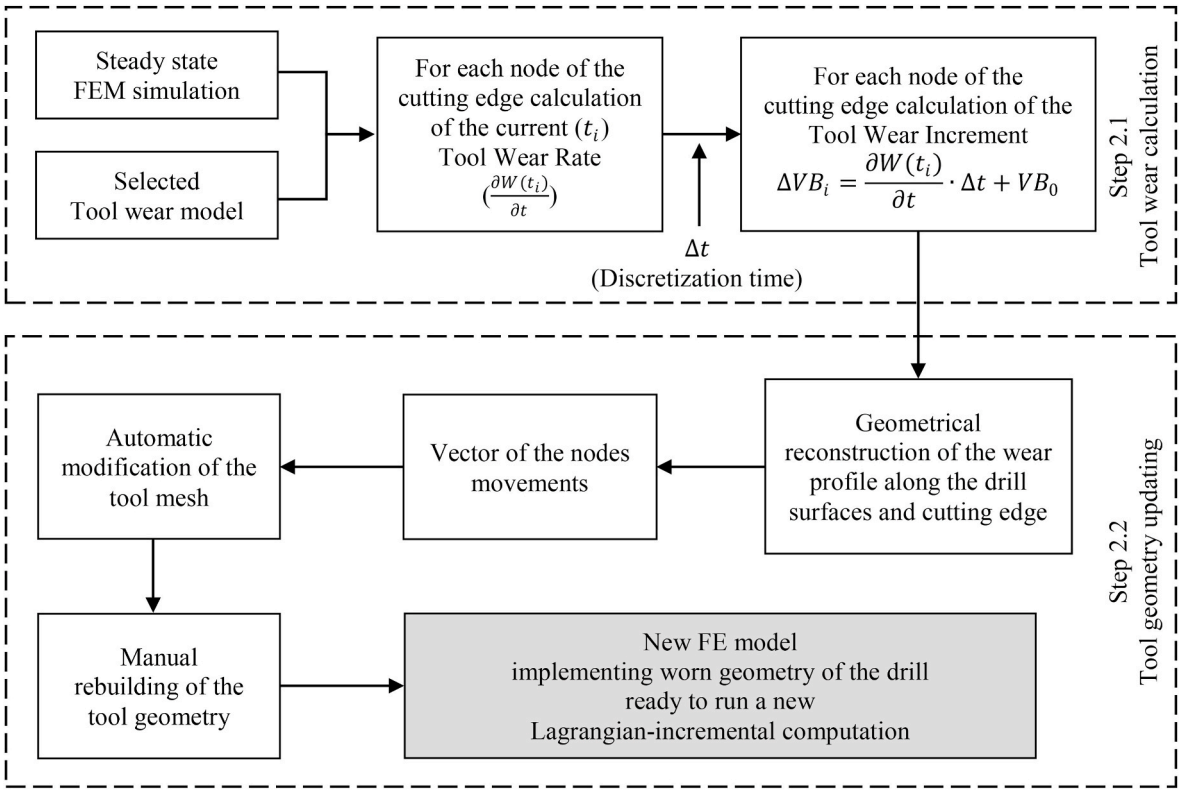

Fig. 5. Flowchart of the subroutine algorithm for tool wear calculation and tool geometry updating.

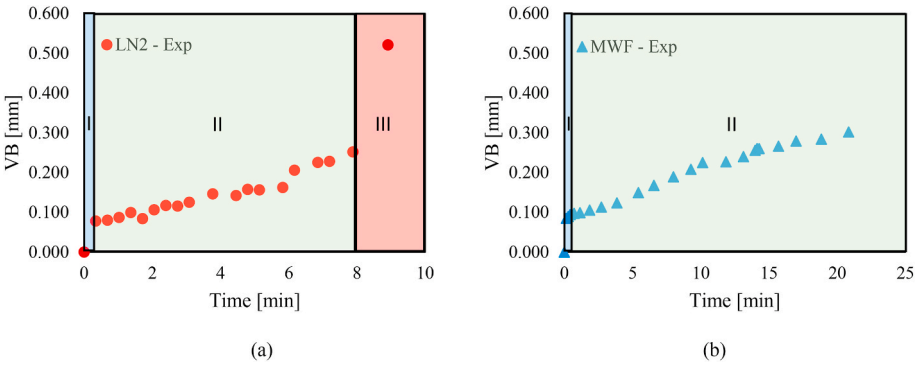

Fig. 6. Tool flank wear VB versus time diagrams for a) cryogenic cooling and b) MWF [47].

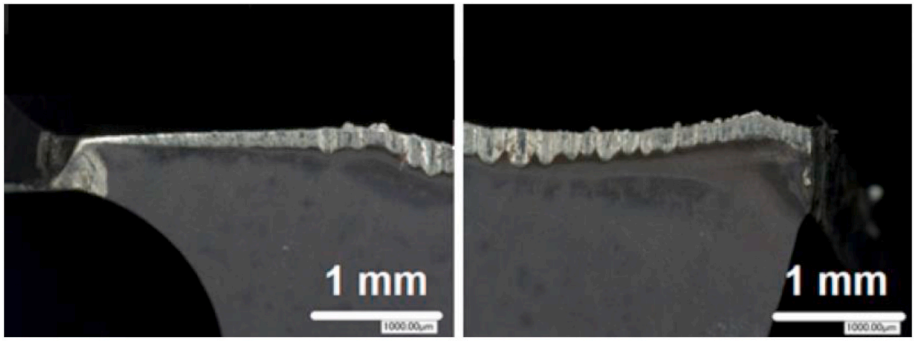

Fig. 7. Flank face of the worn drill (MWF; VB = 0.256 mm) showing the a) chisel edge and the straight part of the cutting edge, b) curved cutting edge and drill periphery.

As reported by Outeiro et al. [47], the normal rake and normal clearance angles (γ and α in Fig. 8a) are varying along the cutting edge depending on the distance from the drill centre (Fig. 8b). Therefore, to correctly update the tool geometry, it is necessary to consider the evolution of these angles along the cutting edge.

For each node of the cutting edge (point C_n in Fig. 8a), along a section orthogonal to the cutting edge and crossing the node, the algorithm identifies the corresponding nodes on the flank face (point A in Fig. 8a), and on the tool rake face (point C in Fig. 8a). Knowing the coordinates of these nodes, the user-routine can calculates the local normal rake (γ) and normal clearance (α) angles.

Both rake and clearance angles, together with ΔVB_i are used to calculate the position (h) of the plane π_3 (Fig. 8a and c). Then, the algorithm determines a local volume, namely local wear volume (LWV), which corresponds to the volume of material loss in the zone surrounding the current node of the cutting edge (C_n). This is done defining two planes π_1 and π_2, orthogonal to the cutting edge and to the plane π_3 and crossing the nodes (C_1 and C_2 in Fig. 8c) neighbouring C_n. The LWV is delimited by the π_1, π_2, π_3 planes, and the rake and flank faces (highlighted volume in Fig. 8c).

In this way, a series of local wear volumes is generated along the tool cutting edge (i.e. one for each node of the cutting edge). The local loss of volume due to wear is finally simulated automatically deleting from the tool mesh all the nodes contained in these local wear volumes. It is evident that the mesh density along the cutting edge affects the accuracy of the simulation. In fact, a high mesh density, which corresponds to a high number of elements and nodes, generates a high number of small LWVs, thus increasing the accuracy of tool wear prediction. Based on the new tool mesh, tool geometry is manually generated in the Deform3D preprocessor.

Once the new tool geometry has been generated, the incremental Lagrangian solver is used to reach the new thermal and mechanical steady-state considering the worn tool geometry. Before running this incremental Lagrangian simulation, a data interpolation between the old and new tool meshes must be done. This operation is necessary to initialise the values of temperature, contact pressure and sliding velocity on the new worn tool mesh.

4. Results and discussion

4.1. Tool wear

Fig. 9 shows the evolution of the predicted tool geometry for both cryogenic (Fig. 9a) and MWF (Fig. 9b) coolant conditions based on the simulated tool wear.

A comparison between experimental and predicted tool flank wear after 21 min of cutting under MWF cooling condition is presented in Fig. 10. The good agreement between experimental and simulated results is evident. The simulation procedure can correctly forecast the tool wear change along the cutting edge. From the chisel edge until the curved part of the cutting edge the tool wear linearly increases, while it remains constant along the curved part of the cutting edge.

Fig. 11 shows the superimposition between the experimental and the simulated tool flank wear VB curves for both cryogenic (Fig. 11a) and MWF (Fig. 11b) cooling conditions. The standard deviation of VB values ranges from 8 μm to 20 μm for FEM data and from 10 μm to 23 μm for experimental data. Observing the graphs of Fig. 11, it is possible to state that a good agreement is obtained between experimental and simulated

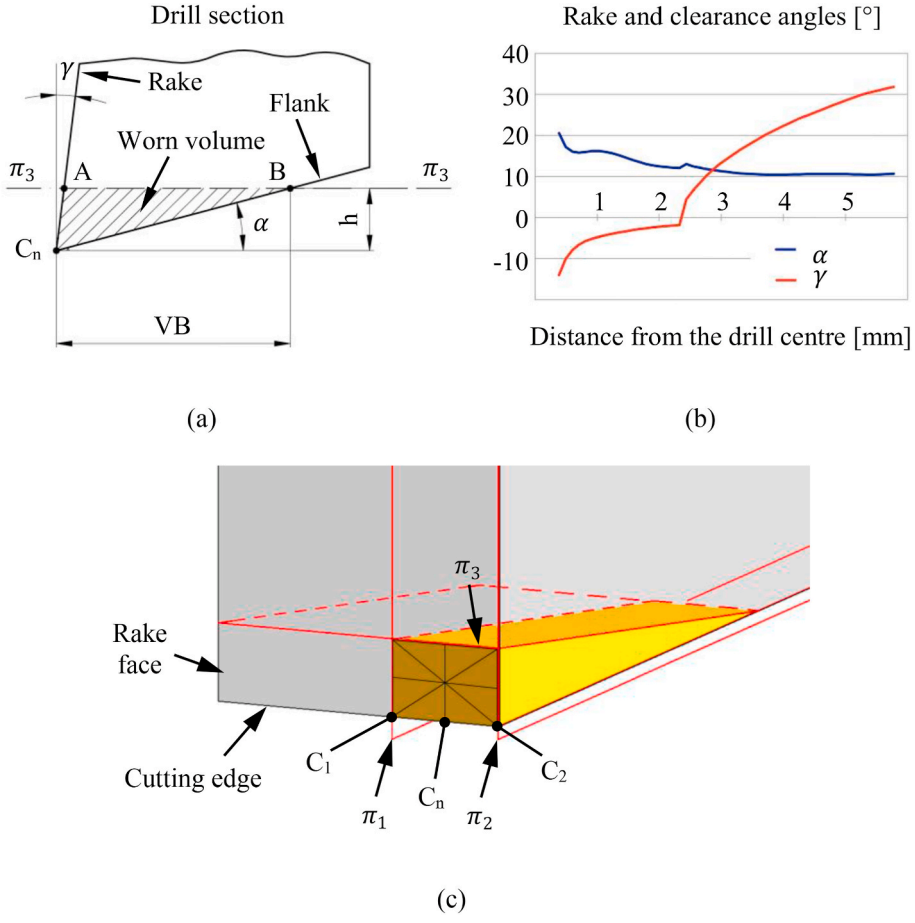

Fig. 8. a) Schematic representation of drill wear at a given section of the cutting edge, b) variation of rake and clearance angles in function of distance from the drill centre [47], and c) local wear volume (LWV).

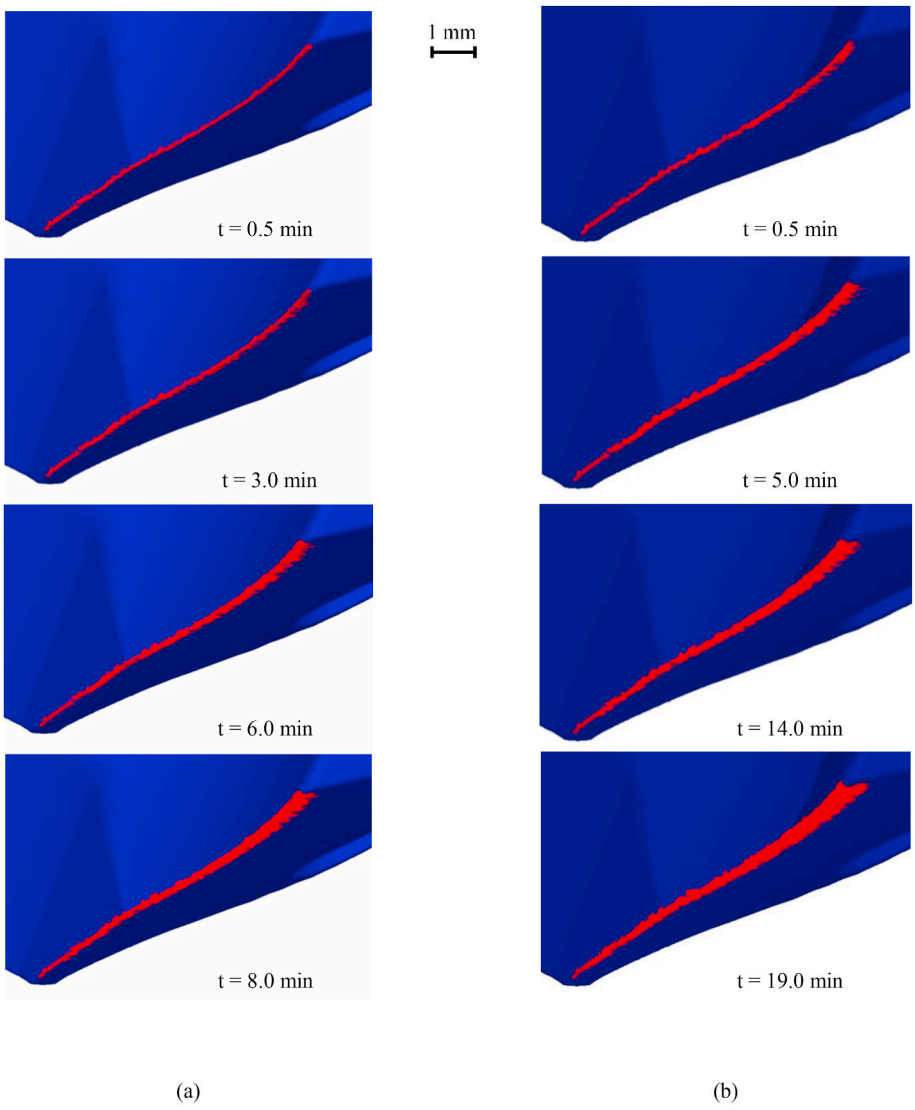

Fig. 9. Tool wear evolution for a) cryogenic and (b) MWF.

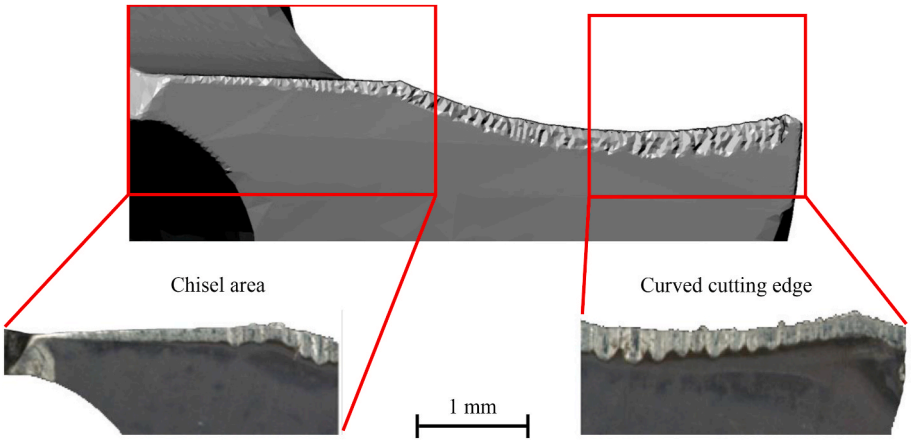

Fig. 10. Simulated (upper) and experimental (bottom) tool wear (MWF, t = 21 min).

results. In fact, the percentage error ranges from 1% to 15% for cryogenic cooling and from 1% to 9% for MWF. Moreover, the maximum gaps between measured and simulated flank wear are very low, being equal to 28 μm for cryogenic cooling (cutting time equal to 2 min), and 27 μm for MWF (cutting time equal to 21 min). Therefore, it is possible to state that the simulations can predict the drill flank wear evolution

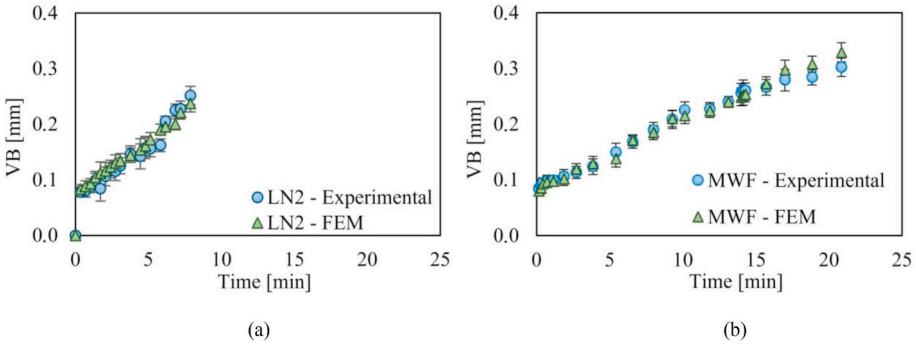

Fig. 11. Comparison between experimental and simulated tool flank wear VB curves for a) cryogenic and b) MWF.

considering the different cooling conditions with high accuracy.

4.2. Torque

Fig. 12 shows the experimental and simulated torque for both cryogenic cooling and MWF conditions at four different flank wear VB values. The four flank wear values selected for the comparison between experimental and simulated outputs, were chosen with the aim of considering cutting times equally distributed along the tool life. Since the torque values are variable, Fig. 12 reports the RMS values. The drilling model showed a good ability to correctly predict the torque. Observing the results presented in Fig. 12, it is evident that the FE model can simulate the increase of the torque with the tool wear. The errors between simulated and experimental torque are low, ranging from 1% to 6% for cryogenic, and from 14% to 20% for MWF.

4.3. Temperature and equivalent stress distributions in the drill

Fig. 13 shows the predicted temperature (Fig. 13a) and stress (Fig. 13b) distributions on the tool. As expected, both temperature and equivalent von Mises stress increase along the cutting edge from the drill centre (chisel edge) to the drill margins. This is due to the increase of the cutting speed from the drill centre to the margins, which generates also an increase of the heat generated by friction. Lower temperature and stress are predicted close to the drill centre, while the maximum values are located close to the periphery of the drill. As a consequence, tool wear should increase from the drill centre to the periphery of the drill, as observed during the experimental tests and presented in Figs. 6 and 10.

The maximum values of the predicted temperature (Fig. 14) and equivalent stress (Fig. 15) were collected at different tool flank wear. The results show that both temperature and stress increase with the tool flank VB wear. Concerning the influence of the cooling conditions, higher temperatures were observed for the MWF cooling (Fig. 14b) when compared to the cryogenic cooling (Fig. 14a). This could be explained by the strongest cooling action of the cryogenic cooling when compared to the conventional MWF [50,57]. In the simulation this is represented by the heat convection coefficients (see h_{conv} values reported in Table 6) characterising both cooling conditions. The very high heat convection coefficient of cryogenic cooling allows to obtain a temperature reduction on the tool higher than 100 °C with respect the MWF cooling condition. On the contrary, the higher stress values are associated to cryogenic cooling (Fig. 15a) when compared to the MWF (Fig. 15b). This could be related with the low temperature of the work material, which causes an increase of the work material strength, due to the reduced thermal softening, and, consequently, higher stresses on the tool.

4.4. Temperature and equivalent stress distributions at the bottom surface of the hole

Fig. 16 shows the predicted temperature (Fig. 16a) and equivalent von Mises stress (Fig. 16b) distributions on the bottom of the hole in drilling using MWF. In particular, Fig. 16b shows chip formation near the cylindrical surface of the hole. Temperatures and equivalent stress increase from the hole centre to the cylindrical surface of the hole. Lower temperature and stresses are located near to the hole centre, while the maximum values to the cylindrical surface of the hole. The knowledge of the temperature and stress distributions in the hole bottom is very important since they affect the surface integrity, in particular the residual stresses. Based on these predicted temperature and stress distributions, it could be expected that the residual stresses at the bottom surface of the hole increase from the hole centre to the cylindrical surface of the hole.

Figs. 17 and 18 present the maximum values of the predicted temperature and equivalent stress for both cryogenic cooling and MWF conditions. Lower temperatures were observed for the cryogenic cooling (Fig. 17a) when compared to the MWF (Fig. 17b). However, lower stress values are obtained by MWF cooling (Fig. 18b) when compared to the cryogenic cooling (Fig. 18a). Like for the tool, the temperature and equivalent stress in the bottom surface of the hole increase with the tool

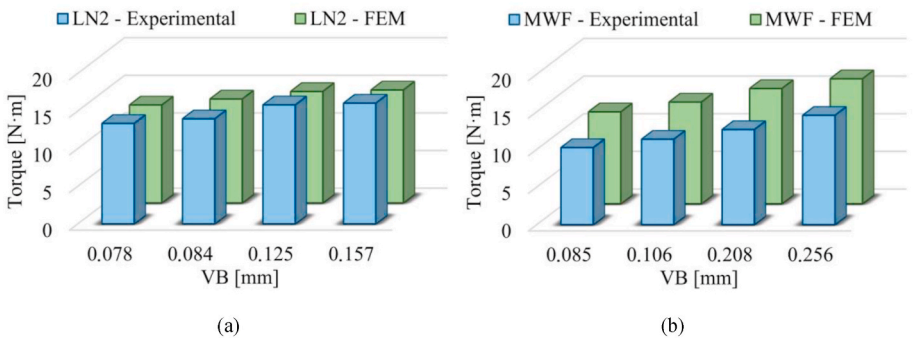

Fig. 12. Comparison between experimental and simulated (FEM) torque for a) cryogenic and (b) MWF.

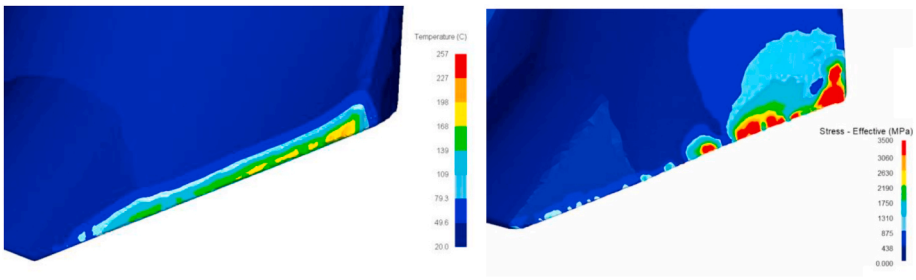

(a) (b)

Fig. 13. Simulated a) temperature and b) equivalent stress distributions in the drill (cryogenic cooling after 6 min of cutting).

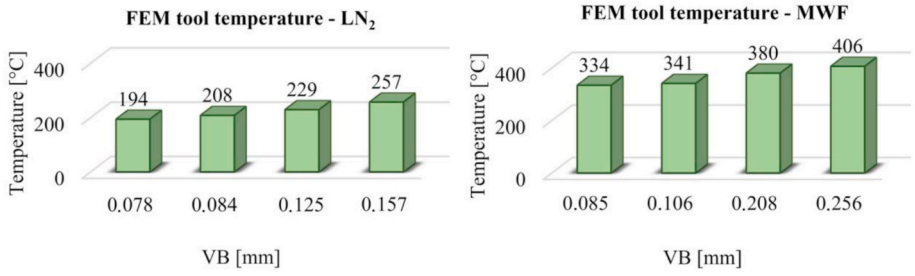

(a) (b)

Fig. 14. Predicted maximum temperatures in the tool vs. tool flank wear VB for a) cryogenic cooling and b) MWF.

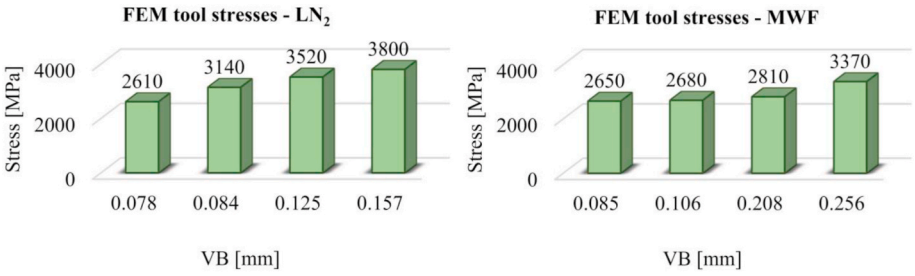

(a) (b)

Fig. 15. Predicted maximum equivalent stresses in the tool vs. tool flank wear VB for a) cryogenic cooling and b) MWF.

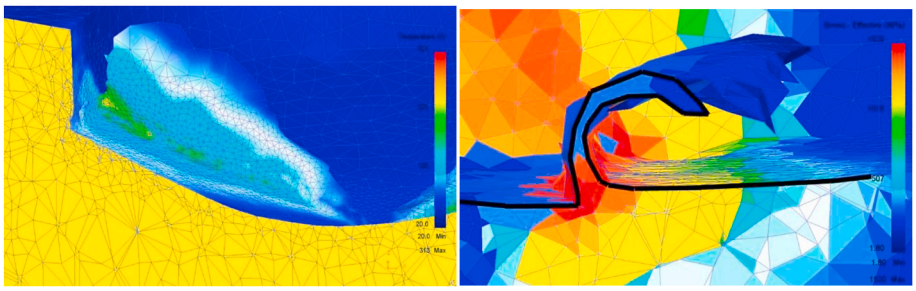

(a) (b)

Fig. 16. Predicted a) temperature distribution and b) equivalent stress distributions (chip section close to the drill periphery) (MWF after 30 s of cutting).

wear. The only exception is for the maximum stress when cryogenic cooling is used (Fig. 18a), where the stress is almost constant. This could be explained considering the low increase of the workpiece temperature (from 218 °C to 274 °C) when the tool wear increases (Fig. 17a).

5. Conclusions

The present research work allowed to develop an innovative simulation procedure to accurately simulate the tool wear in drilling of Inconel 718 nickel-based alloy, under MWF and cryogenic cooling

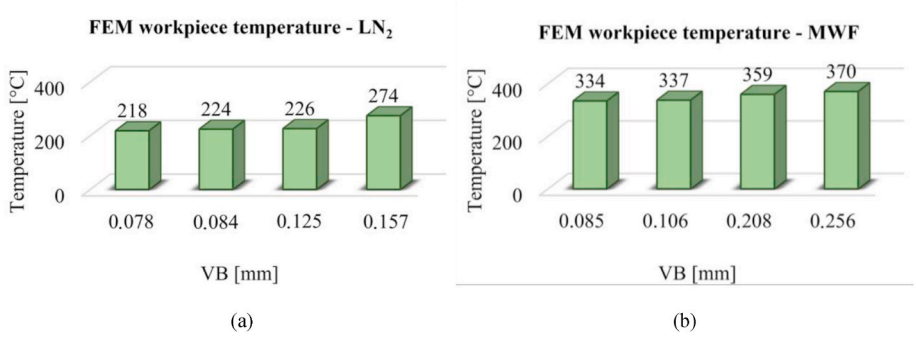

Fig. 17. Predicted maximum temperatures in the bottom of the hole (workpiece) vs. tool flank wear VB for a) cryogenic cooling and b) MWF.

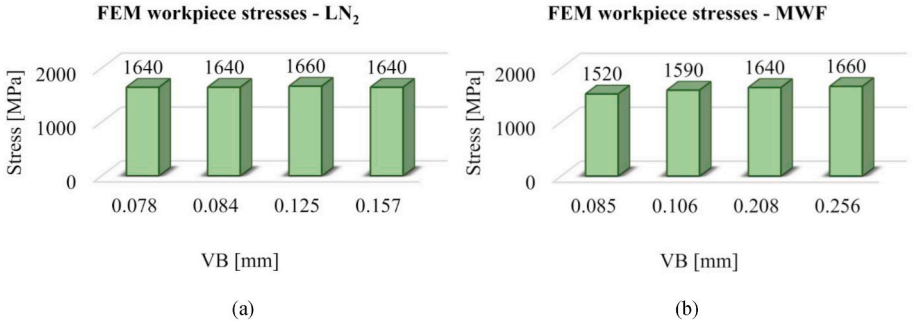

Fig. 18. Predicted maximum equivalent stresses in the bottom of the hole (workpiece) vs. tool flank wear VB for a) cryogenic cooling and b) MWF.

conditions. This procedure is based on a customised user subroutine which combines two numerical formulations (Incremental Lagrangian model and Arbitrary-Lagrangian-Eulerian model to simulate the tool wear.

This procedure was tested on experimental data obtained drilling Inconel 718 under conventional MWF and cryogenic cooling conditions. It was demonstrated that the calibrated procedure can be used to investigate the influence of tool wear on process outputs such as: distribution and equivalent stress distributions in the tool and in the hole.

The procedure is very useful for researchers and workers in cutting field. Several application can be developed starting from it. It can be applied to investigate the influence of tool wear on the surface integrity (including the residual stresses) varying tool materials, workpiece material and lubricant conditions. In this manner, the product quality will be improved. The tool-maker can use this simulating procedure to analysis how the tool wears as the tool geometry changes. Finally, in an Industry 4.0 perspective, the analysis of tool wear can be implemented in artificial neural network with the aim of optimising the tool substitution policy.

Funding

This research did not receive any specific grant from funding agencies in the public, commercial, or not-for-profit sectors.

CRediT authorship contribution statement

A. Attanasio: Conceptualization, Data curation, Formal analysis, Investigation, Methodology, Project administration, Software, Supervision, Visualization, Writing - original draft, Writing - review & editing. **E. Ceretti:** Conceptualization, Methodology, Software, Supervision, Visualization, Writing - original draft, Writing - review & editing. **J. Outeiro:** Conceptualization, Data curation, Methodology, Resources, Validation, Visualization, Writing - original draft. **G. Poulachon:** Conceptualization, Methodology, Project administration, Supervision, Validation, Visualization, Writing - original draft, Writing - review & editing.

Declaration of competing interest

The authors declare that they have no known competing financial interests or personal relationships that could have appeared to influence the work reported in this paper.

Acknowledgments

The Authors wish to thank Ph.D Federico Faini for his technical support during the research.

References

[1] B. Geddes, H. Leon, X. Huang, Superalloys: Alloying and Performance, first ed., ASM International, Novelty (OH), 2010.
[2] S.L. Soo, R. Hood, D.K. Aspinwall, W.E. Voice, C. Sage, Machinability and surface integrity of RR1000 nickel based superalloy, CIRP Ann. - Manuf. Technol. 60 (1) (2011) 89–92.
[3] R. M'Saoubi, J.C. Outeiro, H. Chandrasekaran, O.W. Dillon Jr., I.S. Jawahir, A review of surface integrity in machining and its impact on functional performance and life of machined products, Int. J. Sustain. Manuf. 1 (2008) 203–236.
[4] I.S. Jawahir, E. Brinksmeier, R. M'Saoubi, D.K. Aspinwall, J.C. Outeiro, D. Meyer, D. Umbrello, A.D. Jayal, Surface integrity in material removal processes: recent advances, CIRP Ann. - Manuf. Technol. 60 (2) (2011) 603–626.
[5] R. M'Saoubi, D. Axinte, C. Herbert, M. Hardy, P. Salmon, Surface integrity of nickel-based alloys subjected to severe plastic deformation by abusive drilling, CIRP Ann. - Manuf. Technol. 63 (1) (2014) 61–64.
[6] F. Akhavan Niaki, L. Mears, A comprehensive study on the effects of tool wear on surface roughness, dimensional integrity and residual stress in turning IN718 hard-to-machine alloy, J. Manuf. Process. 30 (2017) 268–280.
[7] R. M'Saoubi, T. Larsson, J.C. Outeiro, Y. Guo, S. Suslov, C. Saldana, S. Chandrasekar, Surface integrity analysis of machined Inconel 718 over multiple length scales, CIRP Ann. - Manuf. Technol. 61 (1) (2012) 99–102.
[8] S.L. Soo, S.A. Khan, D.K. Aspinwall, P. Harden, A.L. Mantle, G. Kappmeyer, D. Pearson, R. M'Saoubi, High speed turning of Inconel 718 using PVD-coated PCBN tools, CIRP Ann. - Manuf. Technol. 65 (1) (2016) 89–92.
[9] B. Lauwers, F. Klocke, A. Klink, A.E. Tekkaya, R. Neugebauer, D. Mcintosh, Hybrid processes in manufacturing, CIRP Ann. - Manuf. Technol. 63 (2) (2014) 561–583.

[10] P. Blau, K. Busch, M. Dix, C. Hochmuth, A. Stoll, R. Wertheim, Flushing strategies for high performance, efficient and environmentally friendly cutting, Procedia CIRP 26 (2015) 361–366.
[11] I.S. Jawahir, H. Attia, D. Biermann, J. Duflou, F. Klocke, D. Meyer, S.T. Newman, F. Pusavec, M. Putz, J. Rech, V. Schulze, D. Umbrello, Cryogenic manufacturing processes, CIRP Ann. - Manuf. Technol. 65 (2) (2016) SS713–736.
[12] G. Poulachon, A. Moisan, I.S. Jawahir, Tool-wear mechanisms in hard turning with polycrystalline cubic boron nitride tools, Wear 250 (1–12) (2001) 576–586.
[13] E. Usui, T. Shirakashi, T. Kitagawa, Analytical prediction of three dimensional cutting process. Part 3. Cutting temperature and crater wear of carbide tool, Trans. ASME 100 (1978) 236–243.
[14] B.M. Kramer, A comprehensive tool wear model, CIRP Ann. - Manuf. Technol. 35 (1) (1986) 67–70.
[15] H. Takeyama, T. Murata, Basic investigations on tool wear, Trans. ASME 85 (1963) 33–38.
[16] A. Molinari, M. Nouari, Modeling of tool wear by diffusion in metal cutting, Wear 252 (2002) 135–149.
[17] S. Shimada, H. Tanaka, M. Higuchi, T. Yamaguchi, S. Honda, K. Obata, Thermo-chemical wear mechanism of diamond tool in machining of ferrous metals, CIRP Ann. - Manuf. Technol. 53 (1) (2004) 57–60.
[18] P.D. Hartung, B.M. Kramer, Tool wear in titanium machining, CIRP Ann. - Manuf. Technol. 31 (1) (1982) 75–80.
[19] H.A. Kishawy, S. Kannan, M. Balazinski, Analytical modeling of tool wear progression during turning particulate reinforced metal matrix composites, CIRP Ann. - Manuf. Technol. 54 (1) (2005) 55–58.
[20] C.Y.H. Lim, S.H. Lim, K.S. Lee, Wear of TiC-coated carbide tools in dry turning, Wear 225–229 (1999) 354–367.
[21] V.P. Astakhov, The assessment of cutting tool wear, Int. J. Mach. Tool Manufact. 44 (2004) 637–647.
[22] R.N. Yong, A.W. Hanna, Finite element analysis of plane soil cutting, J. Terramechanics 14 (3) (1977) 103–125.
[23] T.H.C. Childs, K. Maekawa, Computer-aided simulation and experimental studies of chip flow and tool wear in the turning of low alloy steels by cemented carbide tools, Wear 139 (2) (1990) 235–250.
[24] E. Ceretti, P. Fallböhmer, W.T. Wu, T. Altan, Application of 2D FEM to chip formation in orthogonal cutting, J. Mater. Process. Technol. 59 (1–2) (1996) 169–180.
[25] T. Obikawa, J. Shinozuka, T. Shirakashi, Analytical prediction of cutting performances of grooved rake face tools, J. Jpn. Soc. Precis. Eng. 61 (9) (1995) 1295–1299.
[26] K.D. Bouzakis, N. Vidakis, D. Kallinikidis, T. Leyendecker, G. Erkens, R. Wenke, H. G. Fuss, Fatigue failure mechanisms of multi- and monolayer physically vapour-deposited coatings in interrupted cutting processes, Surf. Coating. Technol. 108–109 (1998) 526–534.
[27] M. Hashimura, K. Ueda, D. Dornfeld, K. Manabe, Analysis of three-dimensional burr formation in oblique cutting, CIRP Ann. - Manuf. Technol. 44 (1) (1995) 27–30.
[28] Z.C. Lin, Y.Y. Lin, Fundamental modeling for oblique cutting by thermo-elastic-plastic FEM, Int. J. Mech. Sci. 41 (8) (1999) 941–965.
[29] P.J. Arrazola, T. Özel, D. Umbrello, M. Davies, I.J. Jawahir, Recent advances in modelling of metal machining processes, CIRP Ann. - Manuf. Technol. 62 (2) (2013) 695–718.
[30] E. Uhlmann, M. Graf von der Schulenburg, R. Zettier, Finite element modeling and cutting simulation of Inconel 718, CIRP Ann. - Manuf. Technol. 56 (1) (2007) 61–64.
[31] G. Liu, C. Huang, R. Su, T. Özel, Y. Liu, L. Xu, 3D FEM simulation of the turning process of stainless steel 17-4PH with differently texturized cutting tools, Int. J. Mech. Sci. 155 (2019) 417–429.
[32] Y. Gao, J.H. Ko, H.P. Lee, 3D coupled Eulerian-Lagrangian finite element analysis of end milling, Int. J. Adv. Manuf. Technol. 98 (1–4) (2018) 849–857, https://doi.org/10.1007/s00170-018-2284-3.
[33] H.S. Patne, A. Kumar, S. Karagadde, S.S. Joshi, Modeling of temperature distribution in drilling of titanium, Int. J. Mech. Sci. 133 (2017) 598–610.
[34] A. Attanasio, E. Ceretti, C. Giardini, 3D FE modelling of superficial residual stresses in turning operations, Mach. Sci. Technol. 13 (3) (2009) 317–337, https://doi.org/10.1080/10910340903237806.
[35] D. Umbrello, R. M'Saoubi, J.C. Outeiro, The influence of Johnson-Cook material constants on finite element simulation of machining of AISI 316L steel, Int. J. Mach. Tool Manufact. 47 (3–4) (2007) 462–470, https://doi.org/10.1016/j.ijmachtools.2006.06.006.
[36] J. Pujana, P.J. Arrazola, R. M'Saoubi, H. Chandrasekaran, Analysis of the inverse identification of constitutive equations applied in orthogonal cutting process, Int. J. Mach. Tool Manufact. 47 (14) (2007) 2153–2161, https://doi.org/10.1016/j.ijmachtools.2007.04.012.
[37] R. M'Saoubi, H. Chandrasekaran, Investigation of the effects of tool micro-geometry and coating on tool temperature during orthogonal turning of quenched and tempered steel, Int. J. Mach. Tool Manufact. 44 (2–3) (2004) 213–224, https://doi.org/10.1016/j.ijmachtools.2003.10.006.
[38] F. Klocke, H.W. Raedt, S. Hoppe, 2D-FEM simulation of the orthogonal high speed cutting process, Mach. Sci. Technol. 5 (3) (2001) 323–340, https://doi.org/10.1081/MST-100108618.
[39] G. Rotella, O.W. Dillon Jr., D. Umbrello, L. Settineri, I.S. Jawahir, Finite element modeling of microstructural changes in turning of AA7075-T651 Alloy, J. Manuf. Process. 15 (1) (2013) 87–95, https://doi.org/10.1016/j.jmapro.2012.09.005.
[40] F. Jafarian, M.I. Ciaran, D. Umbrello, P.J. Arrazola, L. Filice, H. Amirabadi, Finite element simulation of machining Inconel 718 alloy including microstructure changes, Int. J. Mech. Sci. 88 (2014) 110–121.
[41] A. Attanasio, A. Abeni, T. Özel, E. Ceretti, Finite element simulation of high speed micro milling in the presence of tool run-out with experimental validations, Int. J. Adv. Manuf. Technol. 100 (1–4) (2019) 25–35, https://doi.org/10.1007/s00170-018-2678-2.
[42] S. Sai Venkatesh, T.A. Ram Kumar, A.P. Blalakumhren, M. Saimurugan, K. Prakash Marimuthu, Finite element simulation and experimental validation of the effect of tool wear on cutting forces in turning operation, Mech. Mech. Eng. 23 (1) (2019) 297–302.
[43] L.J. Xie, L.-J. Schmidt, C. Schmidt, F. Biesinger, 2D FEM estimate of tool wear in turning operation, Wear 258 (10) (2005) 1479–1490.
[44] A. Attanasio, E. Ceretti, C. Cappellini, C. Giardini, G. Poulachon, Algorithm for tool geometry updating in 3D FEM environment considering the tool wear, Trans. North Am. Manuf. Res. Inst. SME 40 (2012) 21–29.
[45] A. Attanasio, E. Ceretti, A. Fiorentino, C. Cappellini, C. Giardini, Investigation and FEM-based simulation of tool wear in turning operations with uncoated carbide tools, Wear 269 (5) (2010) 344–350.
[46] A. Attanasio, E. Ceretti, S. Rizzuti, D. Umbrello, F. Micari, 3D finite element analysis of tool wear in machining, CIRP Ann. - Manuf. Technol. 57 (1) (2008) 61–64.
[47] J.C. Outeiro, P. Lenoi, A. Bosselut, Thermo-mechanical effects in drilling using metal working fluids and cryogenic cooling and their impact in tool performance, Prod. Eng. 9 (4) (2015) 551–562.
[48] E. Ceretti, C. Giardini, A. Attanasio, L. Filice, S. Rizzuti, D. Umbrello, Diffusion wear modelling in 3D cutting process, Int. J. Mach. Mach. Mater. 6 (1–2) (2009) 95–105, https://doi.org/10.1504/IJMMM.2009.026930.
[49] C. Tahri, P. Lequien, J.C. Outeiro, G. Poulachon, CFD simulation and optimize of LN2 flow inside channels used for cryogenic machining: application to milling of titanium alloy Ti - 6Al - 4V, Procedia CIRP 58 (2017) 584–589.
[50] P. Lequien, G. Poulachon, J.C. Outeiro, J. Rech, Hybrid experimental/modelling methodology for identifying the convective heat transfer coefficient in cryogenic assisted machining, Appl. Therm. Eng. 128 (2018) 500–507.
[51] V.P. Astakhov, Tribology of Metal Cutting, first ed., Elsevier, Oxford (UK), 2006.
[52] A.A. VV, J.P. Davim, Machining Fundamentals and Recent Advances, Springer-Verlag., London, 2008.
[53] E.M. Trent, P.K. Wright, Metal Cutting, fourth ed., Butterworth–Heinemann Editor, Boston, 2000.
[54] Iso 3685, Tool-life Testing with Single-point Turning Tools, 1993.
[55] Iso 8688-1, Tool Life Testing in Milling — Part 1: Face Milling, 1989.
[56] Iso 8688-2, Tool Life Testing in Milling — Part 2: End Milling, 1989.
[57] P. Lequien, G. Poulachon, J.C. Outeiro, Thermomechanical analysis induced by interrupted cutting of Ti6Al4V under several cooling strategies, CIRP Ann. - Manuf. Technol. 67 (1) (2018) 91–94.